

Journal notes on:

Introduction to topological superconductivity

by Francisco Lobo



CONTENTS

Acknowledgments	4
I Introduction to superconductivity theory	5
I. London theory	5
II. BCS theory	5
III. Ginzburg-Landau theory	5
A. Classic type II superconductors	5
B. Josephson effect	5
IV. Time-dependent Ginzburg-Landau theory	5
II Introduction to topological superconductivity	5
V. Concepts of symmetry and topology	5
A. Introduction to CPT symmetries	6
B. Topological invariant in $d = 0$	7
1. Time-reversal symmetry in $d = 0$	8
2. Sublattice symmetry in $d = 0$	9
3. Particle-hole symmetry in $d = 0$	9
4. Combining symmetries	11
C. Introduction to topological invariant in $d > 0$ dimensions	11
VI. One-dimensional models	14
A. Kitaev model	14
1. Majorana modes at a domain wall	17
2. Kitaev ring	18
B. SSH model	18
C. Oreg-Lutchyn model	18
VII. Quantum Hall effects	21
A. Integer quantum Hall effect	21
B. Quantum spin Hall (Kane-Mele) effect	21
C. Quantum anomalous Hall effect	21
D. Fraction Hall effect	21
VIII. Graphene	21
A. Monolayer graphene	21
B. Haldane model	24
C. Bilayer Bernal graphene	24
1. Armchair and Zigzag configurations	26
D. Kekulé modulation	26

ACKNOWLEDGMENTS

I thank Pablo San-Jose and Elsa Prada for their tutoring. I thank César Robles and Carlos Paya for their help. I thank Tiago Antão for useful discussions.

Part I

Introduction to superconductivity theory

I. LONDON THEORY

II. BCS THEORY

III. GINZBURG-LANDAU THEORY

A. Classic type II superconductors

B. Josephson effect

IV. TIME-DEPENDENT GINZBURG-LANDAU THEORY

Part II

Introduction to topological superconductivity

Not a linear story telling of topological superconductivity theory per say, more of a compilation of different models that spark interest due to their topological and superconductive properties. Each section are mostly self contained, having their own bibliography at the start. This chapter closely follows Akhmerov's "Online course on topology in condensed matter" at <https://topocondmat.org/>.

As supplementary material, there is a GitHub repository at <https://github.com/franciscolobo1880/topoSC> where you can check the code that generate the figures of the various models. This is done in *Julia* using the *Quantica.jl* package by Pablo San-Jose, my PhD advisor. Check *Quantica.jl*'s repository and it's tutorial at <https://github.com/pablosanjose/Quantica.jl>.

This chapter closely follows:

- "Introduction to superconductivity" by Tinkham - Dover Publications 9780486435039.

V. CONCEPTS OF SYMMETRY AND TOPOLOGY

The most relevant references used for this section follow:

- Akhmerov's "Online course on topology in condensed matter" at <https://topocondmat.org/>.
- Tiago Antão's Master thesis on "Disorder and Topology in Spin Systems" at <https://repositorium.sdum.uminho.pt>

Topology studies whether objects can be transformed continuously into each other. In condensed matter physics we can ask whether the Hamiltonians of two different systems can be continuously transformed into each other. If that is the case, then we can say that two systems are 'topologically equivalent'.

In order to understand the concept of topology in condensed matter in the simplest way possible let us consider the transformation of a system described by the Hamiltonian \mathcal{H} by the tuning of some external parameter α such that at $\mathcal{H}_i \equiv \mathcal{H}(\alpha = 0)$ is the initial state Hamiltonian and $\mathcal{H}_f \equiv \mathcal{H}(\alpha = 1)$ the final. Understand that the transformation of \mathcal{H} must be physical, meaning that it should be just a matter of point of view. Because of this, not only must \mathcal{H} be an hermitian matrix, i.e $\mathcal{H} = \mathcal{H}^\dagger$ (such that

it has real eigenenergies), but also that any transformation must be isometric (aka norm-preserving) isomorphisms (aka one-to-one mapping). Due to Wigner's theorem these transformations can either be unitary \mathcal{U} or anti-unitary $\bar{\mathcal{U}}$. A unitary transformation between two inner product spaces reads as $\langle \mathcal{U}\varphi|\mathcal{U}\psi\rangle = \langle\varphi|\psi\rangle$ while an anti-unitary transformation reads instead as $\langle \bar{\mathcal{U}}\varphi|\bar{\mathcal{U}}\psi\rangle = \langle\varphi|\psi\rangle^* = \langle\psi|\varphi\rangle$. Of course, any anti-unitary operator can be written as the product of a unitary operator and the complex conjugation operator \mathcal{K} .

Unitary transformations Unitary transformations do not have particularly interesting consequences for topological classification. Consider an Hamiltonian \mathcal{H} with the symmetry constraint $\mathcal{U}^\dagger \mathcal{H} \mathcal{U} = \mathcal{H}$. See that \mathcal{H} commutes with \mathcal{U} meaning that the system has a conservation law, and that the Hamiltonian can be brought to a block-diagonal form

$$\mathcal{H} = \left(\begin{array}{c|c} \mathcal{H}^{(1)} & \\ \hline & \mathcal{H}^{(2)} \end{array} \right), \text{with } \mathcal{H}^{(n)} = \left(\begin{array}{c|c} h_{11} & h_{12} \\ \hline h_{12}^* & h_{22} \end{array} \right). \quad (1)$$

This procedure can be repeated until one runs out of unitary symmetries and is left with an irreducible block of the Hamiltonian, i.e. one which cannot be block diagonalized. In this case, every one of those $\mathcal{H}_i^{(n)}$ Hamiltonians at the n block-diagonal could be continuously deformed into $\mathcal{H}_f^{(n)}$, meaning that they are always topologically equivalent.

A. Introduction to CPT symmetries

One the other hand, anti-unitary transformations do impose constraints on an irreducible Hamiltonian, for example, by forcing it to maintain a (physically) finite energy gap, or to be a real matrix, or to be block off-diagonal. In this case, telling if \mathcal{H}_i and \mathcal{H}_f are topologically equivalent is not trivial. There are three fundamental discrete symmetries: chiral symmetry (CS) \mathcal{C} , parity symmetry \mathcal{P} , time-reversal symmetry (TRS) \mathcal{T} , known collectively as CPT symmetry. In a condensed matter picture, we often refer to the chiral symmetry as being a sublattice lattice and the parity symmetry as a particle-hole symmetry (PHS). Sublattice symmetry means that our system can be naturally split into two interpenetrating sublattices. The Hamiltonian connects only sites from these different sublattices and, as a result, it anticommutes with an operator that distinguishes between them. Particle-hole symmetry means that for every electronic state with energy ε there is a corresponding electron-hole (as in absence of an electron) state, at $-\varepsilon$. Hence, mirroring the electron's occupancy along the Fermi level, meaning that occupied becomes unoccupied and vice versa, the spectrum remains unchanged. Finally, time reversal symmetry means that our system would have behave the same if time flown backwards. In this backward time frame momentums change sign and spins flip.

There is, however, an important detail: both \mathcal{T} and \mathcal{P} are indeed anti-unitary transformations but \mathcal{C} is not. This is because whenever a system has both TRS and PHS there is also a chiral symmetry $\mathcal{C} = \mathcal{P}\mathcal{T}$. This also means that if a system only has either but not both, it cannot have a chiral symmetry. In other words, the presence of any two out of the three symmetries implies that the third is also present. Since the product of two anti-unitary operators is a unitary operator then \mathcal{C} must be unitary. Also, see that if both TRS and PHS are absent, then CS may or may not be present. In these two situations, formally known as *classes*, there are no anti-unitary symmetries, furthering their classification to *complex* classes.

Another important detail is that for TRS we have that $[\mathcal{H}, \mathcal{T}] = 0$ while for PHS we have that $\{\mathcal{H}, \mathcal{P}\} = 0$. By implication of what we just talked, also $\{\mathcal{H}, \mathcal{C}\} = 0$.

Furthermore, as the next and final note about this symmetries, know that TRS and PHS may come in two separate flavors, depending on whether they square to plus or minus one. So, for example, a system can behave in three ways concerning TRS: (1) it does not have TRS, (2) it has it and $\mathcal{T}^2 = +1$ (3) it has it and $\mathcal{T}^2 = -1$. On the other hand, the chiral symmetry only comes in one flavor, $\mathcal{C}^2 = +1$. Due to flavor combinations we find a total of 10 distinct symmetry classes displayed in Fig.(1). The classifications \mathbb{Z} , $2\mathbb{Z}$ and \mathbb{Z}_2 on the left are to be introduced in the following examples.

class	C	P	T	$d = 0$	1	2	3
A				\mathbb{Z}		\mathbb{Z}	
AI			1	\mathbb{Z}			
AII			-1	$2\mathbb{Z}$		\mathbb{Z}_2	\mathbb{Z}_2
AIII	1				\mathbb{Z}		\mathbb{Z}
BDI	1	1	1	\mathbb{Z}_2	\mathbb{Z}		
C		-1				$2\mathbb{Z}$	
CI	1	-1	1			$2\mathbb{Z}$	
CII	1	-1	-1		$2\mathbb{Z}$	\mathbb{Z}_2	
D		1		\mathbb{Z}_2	\mathbb{Z}_2	\mathbb{Z}	
DIII	1	1	-1	\mathbb{Z}_2	\mathbb{Z}_2	\mathbb{Z}	

Figure 1. Symmetry periodic table. For more details on this table, for example, on how to go from $d = 0$ to $d > 0$ by adding and removing symmetries and it's Boot clock patterns see Akhmerov's "10 symmetry classes and the periodic table of topological insulators" at https://topocondmat.org/w8_general/classification.html.

It is important to have in mind that CPT symmetries may not be the only symmetries at play. Although these are the fundamental symmetries, if one works within a condensed matter framework, the underlying lattice will provide additional, often spatial, symmetries. These include, for example point group symmetries—inversion, mirror, and rotational symmetries—, and space group symmetries—translation, glide, or screw symmetries of the entire crystal lattice. Point group symmetries protect additional degeneracies or enforce selection rules that are not captured by the non-spatial discrete symmetries alone, for example, a mirror symmetry in a crystal that protects gapless modes on certain surfaces or edges that are invariant under reflection. One the other hand space group symmetries constrain the electronic band structure and can lead to phenomena like Dirac or Weyl points that interact with the superconducting pairing.

B. Topological invariant in $d = 0$

In order to study the effects of these symmetries, let us imagine a panoply of different systems and their energy spectrums as a function of α . Moreover, let us count the number of levels below zero energy (defined at the Fermi level ε_F) at each different α , denoting it with Q . This will be our topological invariant prototype. If Q is the same in the initial and final system and did not change along the tuning of α then there must be a continuous transformation Hamiltonian which does not close the gap. One the other hand, if Q changes then the system are *not* topologically equivalent as it would be needed to close the (physically real) gap. Hence, such a crossing changes the topological invariant, dubbed topological phase transition.

For all the examples that follow we assume a zero-dimensional ($d = 0$) system. In a condensed matter realization this could be, for instance, a quantum dot interaction with all kinds of external systems. This will become

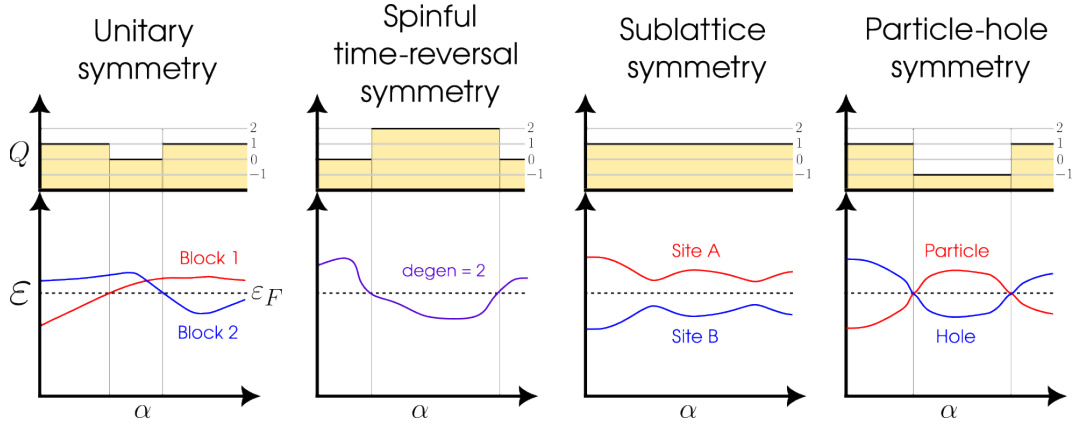


Figure 2. Kitaev chain Majorana modes pairing possibilities tbh I still don't fully understand why I can't just change the Fermi energy? I mean, for the spinful TRS I could only get 0 or 2 still. Does the spectrum of the CS and PHS just translate along with ε_F while the unitary does not?

1. Time-reversal symmetry in $d = 0$

Time-reversal symmetry is represented by an anti-unitary operator, and as such it can always be written as the product $\mathcal{T} = U\mathcal{K}$ with U an unitary matrix and \mathcal{K} complex conjugation. A real Hamiltonian is a manifestation of time-reversal symmetry.

Spinless case

For example, for a spinless system we have $\mathcal{T} = \mathcal{K}$ and thus $\mathcal{T}\mathcal{H}\mathcal{T}^{-1} = \mathcal{H}^* = \mathcal{H}$ is a real matrix. In this case the TRS flavor is positive i.e. $\mathcal{T}^2 = +1$. Still, this case is also not interesting because is not different from the previous one, the different energy levels move and the topological invariant changes by one when one of them crosses zero. In this trivial case the topological invariant is an integer number, $Q = 0, \pm 1, \pm 2, \dots \in \mathbb{Z}$. I mean, it should be \mathbb{N} no? How would the negative numbers appear?

Spinful case

There is, however, a very important case where time-reversal symmetry makes a real difference. For a 1/2-spin system we the time-reversal operator reads $\mathcal{T} = i\sigma_y\mathcal{K}$ with $\sigma_y = [0 \ -i; +i \ 0]$ the 2nd Pauli matrix (we reserve σ for Pauli matrices in spin orbital space). In this case the flavor is negative, i.e. $\mathcal{T}^2 = -1$, and $\mathcal{T}\mathcal{H}\mathcal{T}^{-1} = \sigma_y\mathcal{H}^*\sigma_y = \mathcal{H}$ meaning that every energy eigenvalue ε is doubly degenerate. This happens because both the electrons with spin up or down have the same eigenenergy. This doubly degeneracy is often refer to as Kramers' degeneracy. Such a Hamiltonian would read in matrix form as

$$\mathcal{H} = \left(\begin{array}{c|c} \varepsilon_1 \mathbb{1} & M \\ \hline M^\dagger & \varepsilon_2 \mathbb{1} \end{array} \right) = \left(\begin{array}{cc|cc} \varepsilon_1 & 0 & m_{11} & m_{12} \\ 0 & \varepsilon_1 & -m_{12}^* & m_{11}^* \\ \hline m_{11}^* & -m_{12} & \varepsilon_2 & 0 \\ m_{12}^* & m_{11} & 0 & \varepsilon_2 \end{array} \right). \quad (2)$$

with $\varepsilon_1, \varepsilon_2$ real numbers.

We can see the consequences of Kramers' degeneracy on the band spectrum versus α in Fig.(2). While the spectrum looks quite similar to the previous ones, whenever a line crosses zero energy, our topological invariant makes a jump of two, and not one! In this case, time-reversal symmetry constrains the topological invariant to only take even values, $Q = 0, \pm 1, \pm 2, \dots \in 2\mathbb{Z}$. This is an example of how topological properties can be influenced by discrete symmetries.

2. Sublattice symmetry in $d = 0$

We just saw that time-reversal symmetry can forbid the topological invariant to take a certain set of values. We now study another case where a symmetry changes the topological properties dramatically.

Let's now take a system where we can split all the degrees of freedom into two groups—group A and group B —, such that the Hamiltonian only has nonzero matrix elements between two groups, and not inside each group. This situation arises naturally when the a given lattice has two sublattices. For example, for hexagonal boron nitrate (hBN) we can distinguish these sublattices as the boron and nitrogen sites respectively. The matrix of such an Hamiltonian would read

$$\mathcal{H} = \left(\begin{array}{c|c} M & \\ \hline M^\dagger & \end{array} \right) = \left(\begin{array}{cc|cc} 0 & 0 & m_{11} & m_{12} \\ 0 & 0 & m_{21} & m_{22} \\ \hline m_{11}^* & m_{21}^* & 0 & 0 \\ m_{12}^* & m_{22}^* & 0 & 0 \end{array} \right). \quad (3)$$

See that $\eta_z \mathcal{H} \eta_z = -\mathcal{H}$ where $\eta_z = [+1 \ 0 ; 0 \ -1]$ is the 3rd Pauli matrix (we reserve η for Pauli matrices in sublattice orbital space). This immediately means that if $\Psi = [\psi_A ; \psi_B]^T$ is an eigenvector of the Hamiltonian with energy ε , then $[\psi_A ; -\psi_B]^T$ is an eigenvector with energy $-\varepsilon$. A symmetric spectrum is the consequence of sublattice symmetry as seen in Fig.(2). This means that Q always stays constant and that we can always deform Hamiltonians with sublattice symmetry without closing the gap. This indicates that an extra symmetry, such as this one, may render the topology of a system as trivial.

3. Particle-hole symmetry in $d = 0$

Another symmetry that has a strong influence on topology is the particle-hole symmetry, showing up in superconducting systems. As we saw in BCS theory, a superconductor will create(annihilate) pairs of electrons by breaking(forming) Cooper pairs costing a pairing energy of Δ to the system.

Let us consider that the dynamics of the electrons is described by the an hermitian H matrix while the pair creation and annihilation is described by an antisymmetric Δ matrix. Understand that Δ must antisymmetric just because because the fermion operators anticommute. The Hamiltonian describing the full system reads

$$\mathcal{H} = \left(\begin{array}{c|c} H & \Delta \\ \hline -\Delta^* & -H^* \end{array} \right) = \left(\begin{array}{cc|cc} h_{11} & h_{12} & 0 & \Delta \\ h_{12}^* & h_{22} & -\Delta & 0 \\ \hline 0 & -\Delta^* & -h_{11}^* & -h_{12}^* \\ \Delta^* & 0 & -h_{12} & -h_{22}^* \end{array} \right) \quad (4)$$

and is know as the Bogoliubov-de Gennes (BdG) Hamiltonian. Moreover, we now double the amount of degrees of freedom in the system by defining a Nambu spinors

$$\check{c}_i^\dagger = \begin{pmatrix} c_i^\dagger & c_i \end{pmatrix} \quad \text{and} \quad \check{c}_i = \begin{pmatrix} c_i \\ c_i^\dagger \end{pmatrix} \quad (5)$$

such that we can write

$$\check{\mathcal{H}} = \frac{1}{2} \check{c}^\dagger \mathcal{H} \check{c}.$$

This definitions indicates that the Bogoliubov-de Gennes Hamiltonian acts not only on electrons but also on an extra mirror set comprised of eletron-holes. Since holes are related to the electrons, \mathcal{H}

automatically inherits that extra symmetry. This symmetry exchanges electrons with holes, and has an anti-unitary operator $\mathcal{P} = \tau_x \mathcal{K}$ with $\tau_x = [0 \ 1 ; 1 \ 0]$ the 1st Pauli matrix (we reserve σ for Pauli matrices in spin orbital space) and (as before) \mathcal{K} complex conjugation. Hence we have that $\mathcal{P}\mathcal{H}\mathcal{P}^{-1} = -\mathcal{H}$. For this specific case it's flavor is positive, i.e $\mathcal{P}^2 = +1$. Indeed, for every eigenvector $\Psi = [u; v]^T$ with energy ε , there will be a particle-hole symmetric eigenvector $\mathcal{P}\Psi = [v^*; u^*]^T$ with energy $-\varepsilon$. As clearly seen in Fig.(2), because of the minus sign in the particle-hole symmetry, the spectrum of \mathcal{H} must be mirrored around zero energy, that is, the Fermi level).

Fermionic parity switches

See that this spectrum mirroring was also the case for sublattice symmetry however, in this case, energy levels do not repel around zero energy, so that crossings at zero energy appear. Unlike in the case of sublattice symmetry, a pair of $\pm\varepsilon$ energy levels does not corresponds to two distinct quantum states, but to a single quantum state. This quantum state is a coherent superposition of electrons and holes, a so called Bogoliubov quasiparticle. It has an excitation energy ε , and it is created by an operator $\gamma^\dagger = uc^\dagger + vc$. Populating the partner state at energy ε is the same as emptying the positive energy state.

In general a crossing between energy levels happens in the presence of a conserved quantity. While the mean-field Hamiltonian of a superconductor does not conserve the number of particles, it conserves the parity of this number. In other words, forming and breaking Cooper pairs does not affect whether the superconducting contains an even or odd number of electrons so fermion parity is a conserved quantity (provided that isolated electrons do not enter or leave the system). Fermion parity, however, is a many-body quantity, which cannot be directly described in terms of the single particle picture of the BdG Hamiltonian. This is why we had to double the number of degrees of freedom by hand. When a pair of levels crosses zero energy, the excitation energy ε of the Bogoliubov quasiparticle changes sign and it becomes favorable to add(remove) a Bogoliubov quasiparticle. In other words, at each crossing the fermion parity in the ground state changes from even to odd (or vice versa), meaning that these crossings are fermion parity switches.

The Pfaffian invariant

Since the ground state fermion parity is preserved by the superconducting Hamiltonian if there are no Bogoliubov quasiparticles crossing zero energy, the ground state fermion parity is the topological invariant of this system. It is clear however that this invariant is of a different nature than the one of the non-superconducting systems, which is given by the number Q of negative eigenvalues of the Hamiltonian. The latter cannot change for a BdG Hamiltonian, which has a symmetric energy spectrum, and hence it is not suitable to describe changes in fermion parity. For this kind of systems the actual topological invariant is called the *Pfaffian* and will either take the value $Q = \pm 1 \in \mathbb{Z}_2$ at every zero-energy crossing. Its rigorous definition is not really that important for our sake so we take a simpler approach.

In order to introduce the Pfaffian invariant, we start by making a basis transformation $\mathcal{H}'_{\text{BdG}} = \mathcal{U}\mathcal{H}_{\text{BdG}}\mathcal{U}^\dagger$ that makes the Hamiltonian an skew-symmetric matrix, i.e $\mathcal{H}^T = -\mathcal{H}$. We do this because the eigenvalues of antisymmetric matrices always come in pairs, i.e $\pm\varepsilon_n$. Further reasoning will become apparent as we go. Such a transformation is

$$\mathcal{H}'_{\text{BdG}} = \frac{1}{2} \begin{pmatrix} 1 & 1 \\ i & -i \end{pmatrix} \mathcal{H}_{\text{BdG}} \begin{pmatrix} 1 & 1 \\ i & -i \end{pmatrix} = \frac{1}{2} \begin{pmatrix} H - H^* + \Delta - \Delta^* & |i(-H - H^* + \Delta + \Delta^*)| \\ i(+H + H^* + \Delta + \Delta^*) & H - H^* - \Delta + \Delta^* \end{pmatrix}$$

Indeed, because H is Hermitian then $H - H^*$ is antisymmetric and $H + H^*$ is symmetric, i.e $\mathcal{H}^T = \mathcal{H}$; since Δ is antisymmetric then $\mathcal{H}'_{\text{BdG}}$ is also antisymmetric. In its diagonalized form the determinant of this matrix is just the product of the pairs of eigenenergies, i.e $\det(\mathcal{H}) = \prod_n (-\varepsilon_n^2)$. The key feature of the Pfaffian is revealed when taking now the square root of the determinant $\text{Pf}(\mathcal{H}) = \sqrt{\det(\mathcal{H})} = \pm \prod_n i\varepsilon_n$. See that it is defined in such a way that the sign of the product is uniquely defined. At a fermion parity switch a single ε_n changes sign, so the Pfaffian changes sign as well while the determinant

stays the same. We then define the actual topological invariant as

$$Q_{\text{BdG}} = \text{sign} [\text{Pf}(i\mathcal{H})],$$

where we have included a factor of i just that the Pfaffian is a real number, such that at Q_{BdG} changes its value from $+1$ to -1 at every zero-energy crossing. This means that it is the correct expression for the ground state fermion parity and for the topological invariant. As some sort of intuition, you can think of it as if the number of holeonic levels below zero energy counts negatively to the overall positive electronic levels.

4. Combining symmetries

Particle-hole and spinful time-reversal symmetry

Take a system that has both particle-hole symmetry (PHS) and spinful time-reversal symmetry (TRS) described by the Hamiltonian \mathcal{H} . Let us take an intuitive approach to the band spectrum analysis. By PHS we know that an electronic band is equivalent to a negative holeonic band. On the other hand, by spinful TRS we know that there is Kramer degeneracy. Hence, since a PHS holeonic band counts as negative to the number of bands below zero energy we will always end up with Q being even and changing sign at a crossing. *This is wrong but can't see the flaw in logic. I mean, looking at the table I can see that $P^2 = 1$ and $T^2 = -1$ gives me no constrain on Q and thus trivial topology.*

C. Introduction to topological invariant in $d > 0$ dimensions

In higher dimensional system the discrete energy levels of a $d = 0$ system are replaced by continuous energy bands defined along the Brillouin zone. In these higher dimensions the topological invariant cannot be defined merely as counting levels below the Fermi energy or by tracking sign changes of the Pfaffian in superconducting systems. Instead, the central theme of $d > 0$ dimensional band topology lies in the concept of geometric phases.

As an illustrative example of the concepts to come, consider a vector placed at the earth's north pole, always pointing in the tangent direction to the surface. If one translates the vector to the equator along a meridian, then along the equator for some distance, and back to the north pole, the vector's orientation will have changed relative to how it started by some angle. This angle is called the holonomy. The origin of non-trivial band topological properties is not so different from this example, with the crucial replacement of the vector by a Hamiltonian $\mathcal{H}(\boldsymbol{\alpha})$ depending on a set of parameters $\boldsymbol{\alpha} = (\alpha_1, \dots, \alpha_N)$, and the earth a manifold (topological space that locally resembles Euclidean space near each point) spanned by those parameters. In the context of Hamiltonians, holonomy manifests as the acquisition of additional geometric phases by the eigenstate of $\mathcal{H}(\boldsymbol{\alpha})$ as the parameter space manifold is traversed. More concretely, in band topology, $\boldsymbol{\alpha}$ is taken to be the momenta $\mathbf{k} = (k_1, \dots, k_d)$, with d the space dimensions, together with a set of additional tunable parameters (chemical potential, electric field, Zeeman, integrated out pairing, etc, etc...), and the eigenstate's additional geometric phase is the so-called Berry phases (we will further explore this later concept in just a moment). In this context, the restriction that evolution is adiabatic simply means that the system must remain in a situation where energy bands do not cross, i.e. the system must be gapped.

The idea is that if the parameters $\boldsymbol{\alpha}$ are varied adiabatically, then at each subsequent value of $\boldsymbol{\alpha}$, eigenstates of one set of parameters are smoothly deformed into another set. This is the content of the adiabatic theorem, which states that in the case of adiabatic evolution of the parameters along a curve $\boldsymbol{\alpha}(t)$, the Schrodinger equation

$$-i\hbar\partial_t |\psi_n(\boldsymbol{\alpha}(t))\rangle = \varepsilon_n(\boldsymbol{\alpha}(t)) |\psi_n(\boldsymbol{\alpha}(t))\rangle \quad (6)$$

is obeyed instantaneously. Here $|\psi_n(\boldsymbol{\alpha}(t))\rangle$ represents the eigenstate of the Hamiltonian $\mathcal{H}(\boldsymbol{\alpha}(t))$ in the n th band with energy $\varepsilon_n(\boldsymbol{\alpha}(t))$. Now, generically, due to the structure of the Schrodinger equation, and the normalization of states, a single degree of freedom exists, which can change the eigenstate as it is moved along the parameter space $\boldsymbol{\alpha}(t)$. This corresponds to a phase denoted by $\theta(t)$, such that the state can be decomposed as

$$|\psi(\boldsymbol{\alpha}(t))\rangle = e^{i\theta(t)/\hbar} |\phi(\boldsymbol{\alpha}(t))\rangle. \quad (7)$$

A short calculation performed by plugging this form of the state into the Schrodinger equation on both sides, and acting with $\langle\psi(\boldsymbol{\alpha}(t))|$ on the left is enough to solve for the phase $\theta(t)$. One obtains

$$\theta(t) = \int_0^{t'} dt \left[\varepsilon(\boldsymbol{\alpha}(t)) + \frac{i}{\hbar} \langle\phi(\boldsymbol{\alpha}(t))| \partial_t |\phi(\boldsymbol{\alpha}(t))\rangle \right] \quad (8)$$

There are two contributions to the phase acquired by the eigenstate under adiabatic evolution. The first term is the familiar dynamical phase $\theta_D(t)$, which is acquired from evolving in time in the Hilbert space. However, a second term appears, namely

$$\gamma(t) = \frac{i}{\hbar} \int_0^{t'} dt \langle\phi(\boldsymbol{\alpha}(t))| \partial_t |\phi(\boldsymbol{\alpha}(t))\rangle$$

which is called the geometrical phase or Berry phase. This phase can be calculated via the aforementioned time integral, or equivalently by integrating over the curve \mathcal{C} spanned in the parameter space α during the adiabatic evolution, reading

$$\gamma_{\mathcal{C}} = \int_{\mathcal{C}} d\boldsymbol{\alpha} \frac{i}{\hbar} \langle\phi(\boldsymbol{\alpha})| \nabla_{\boldsymbol{\alpha}} |\phi(\boldsymbol{\alpha})\rangle \equiv \int_{\mathcal{C}} d\boldsymbol{\alpha} \mathbf{A}(\boldsymbol{\alpha}) \quad (9)$$

with $A(\alpha)$ the so called Berry connection.

The Berry connection plays the same role in adiabatic evolution as the vector potential in electromagnetism, and indeed, much like in the latter theory, this connection can be used to construct a curvature tensor. In the context of electromagnetism, the curvature tensor is nothing but the electromagnetic tensor $F_{\mu\nu}$, while in the context of the adiabatic evolution of quantum systems, it is given the special name of Berry curvature $\Omega_{\mu\nu}$. Explicitly, this Berry curvature reads

$$\Omega_{\mu\nu}(\boldsymbol{\alpha}) = \frac{\partial}{\partial \alpha^\mu} A_\nu(\boldsymbol{\alpha}) - \frac{\partial}{\partial \alpha^\nu} A_\mu(\boldsymbol{\alpha})$$

One often considers the dual pseudo-vector to this tensor, this is $\Omega_{\mu\nu} = \varepsilon_{\mu\nu\xi} \Omega^\xi$ with $\varepsilon_{\mu\nu\xi}$ the Levi-Civita symbol, and calls that the Berry curvature instead. This quantity is analogous to the magnetic field $\mathbf{B} = \nabla \times \mathbf{A}$. Another similarity between electromagnetism and these concepts is that the Berry connection, like the magnetic vector potential, is defined only up to a gauge choice. This makes it so the Berry phase is only well defined if closed curves \mathcal{C} in the parameter space are considered.

As a final summary, information about the topology of the target space of $\mathcal{H}(\boldsymbol{\alpha})$ is acquired by integrating the Berry connection or curvature over the entire Brillouin zone, or in other words, the holonomy of the Hamiltonian as the Brillouin zone is traversed is sensitive to the band-topology. The integration of this Berry curvature yields quantities called topological invariants which are analogous to the Winding number of the Aharonov-Bohm effect (see the example below). In this $d > 0$ context, one can also refer to the topological invariants as Chern number.

A fundamental consequence of having a well-defined topological invariant in $d > 0$ is the so-called bulk-boundary correspondence. This principle asserts that nontrivial topological properties in the bulk of a material inevitably give rise to robust, gapless modes at its boundaries, whether along edges in 2D or surfaces in 3D. One can intuitively see why this should be the case by noting that at the boundary of a topological non-trivial system there is only vacuum, a topological trivial system. This means that, at this boundary, the topological invariant must change from something non-zero to zero which is only possible if the gap closes. This gives rise to emergent gapless edge state which are protected against perturbations that do not close the bulk gap.

Example: Aharonov-Bohm effect

As a predecessor to the topological band theory, we now introduce the reader to an electromagnetism examples known as the Aharonov-Bohm (A-B) effect as a starting point to understanding the Berry phase, connection, curvature in more detail.

Consider an electron whose movement is restricted to the xOy place where an infinitely thin and long solenoid pierces through it at its center. Inside the solenoid an electric current flow inducing a magnetic field $\mathbf{B} = B\hat{z}$ such that a magnetic flux ϕ flows penetrates the the plane of motion of the electron. Although there exists no field or flux outside the solenoid, a magnetic vector potential \mathbf{A} permeates all space. Now, note that the electron wandering the plane will actually be affected by the vector potential, in that the Hamiltonian describing it will have the form

$$\mathcal{H}(\mathbf{r}) = \frac{\hbar^2}{2m} (\nabla - e\nabla \cdot \mathbf{A}(\mathbf{r}))^2 \quad (10)$$

with $\mathbf{p} = -i\hbar\nabla$ the momentum operator, e the electron charge and m its mass. In this case, the parameters α can be identified with the actual position of the electron \mathbf{r} . Since the electron cannot enter the solenoid, which is assumed to be placed at $\mathbf{r} = 0$, its movement is restricted to everywhere except there.

As explain in the previous section, as the electron moves following a curve \mathcal{C} it will acquire a Berry phase, or rather, is in this context, the A-B phase, given by Eq.(9) as

$$\gamma_{\text{A-B}} = \frac{e}{\hbar} \oint_{\mathcal{C}} d\mathbf{r} \mathbf{A}(\mathbf{r}), \quad (11)$$

with \mathbf{A} being not the general Berry connection but the actual physical vector potential. The A-B phase, in some sense, measures the inability of making a continuous gauge choice for the magnetic vector potential in a punctured plane. The presence of the puncture hole makes it so a discontinuity along a branch cut is a mathematical necessity, and as a result, if an electron loops around the hole, it will acquire a non-trivial phase, dependent only on the number of times it goes around the hole (see Fig. 3). For this reason, it is said that the A-B phase is a topological quantity, depending only on the topology of the electron's trajectory, namely on a quantity called the winding number.

Alternatively, through the usage of Stoke's theorem, it is simple enough to compute the A-B phase as being proportional to the magnetic flux, this is

$$\gamma_{\text{A-B}} = \frac{e}{\hbar} \iint d\mathcal{S} \cdot \mathbf{B} = \frac{e}{\hbar} W\phi$$

enclosed by the trajectory's area \mathcal{S} , where $W \in \mathbb{Z}$ counts the number of loops the electron makes around the solenoid. It's precisely this quantity that corresponds precisely to the winding number.

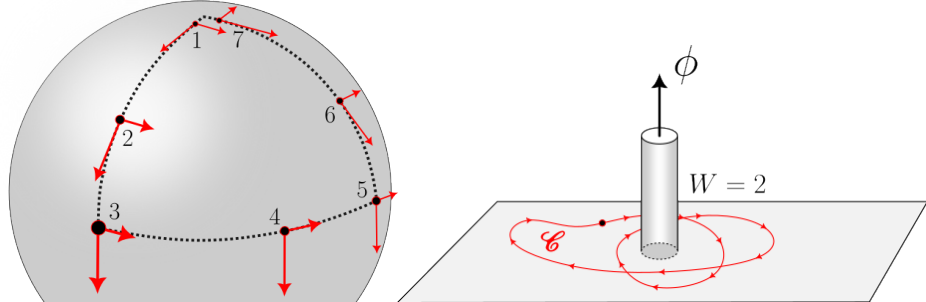


Figure 3. (a) Holonomy, (b) Aharonov-Bohm effect

VI. ONE-DIMENSIONAL MODELS

A. Kitaev model

The most relevant references used for this section follow:

- Kitaev's "Unpaired Majorana fermions in quantum wires" - Phys.-Usp. 44 131
- Akhmerov's "Online course on topology in condensed matter" at <https://topocondmat.org/>.

The *Kitaev chain* or *Kitaev–Majorana chain* is a toy model for a topological superconductor using a 1D hybrid (semiconductor+superconductor) nanowires featuring Majorana bound states. It consists of a 1D linear lattice of N site and spinless fermions at zero temperature, subjected to nearest neighbor hoping interactions. The real-space tight-binding Hamiltonian describing such model reads

$$H = \mu \sum_{i=1}^N \left(c_i^\dagger c_i - \frac{1}{2} \right) - t \sum_{i=1}^{N-1} \left(c_{i+1}^\dagger c_i + h.c. \right) + \Delta \sum_{i=1}^{N-1} \left(c_{i+1}^\dagger c_i^\dagger + h.c. \right) \quad (12)$$

with c_i^\dagger (c_i) fermionic creation (annihilation) operators, μ the chemical potential, t the hopping energy and Δ an proximity induced superconducting p -wave pairing.

The objective of this model definition is to be able to have a Majorana bound states on the edges mode. For this, let us engineering the Hamiltonian in such a special way that it is actually possible to separate two Majoranas. Foremost, we define each site n as if it has two sublattices, $s = A$ and $s = B$. We then define Majorana operators relating to the fermionic operators as

$$\gamma_i^A = c_i^\dagger + c_i \quad \text{and} \quad \gamma_i^B = i(c_i^\dagger - c_i) \quad (13)$$

or rather, in the opposite way, as

$$c_i^\dagger = \frac{1}{2}(\gamma_i^A - i\gamma_i^B) \quad \text{and} \quad c_i = \frac{1}{2}(\gamma_i^A + i\gamma_i^B) \quad (14)$$

Indeed, each site can host a fermion or, equivalently, each site hosting two Majorana modes. These Majorana operators are Hermitian $\gamma_i^s = (\gamma_i^s)^\dagger$, unitary $(\gamma_i^s)^2 = 1$ and anticommute as $\{\gamma_i^s, \gamma_j^{s'}\} = 2\delta_{ij}\delta_{ss'}$.

Substituting directly into the Hamiltonian of Eq.(12) the fermionic operators as given by Eqs.(14) we obtain

$$H = -i\mu \frac{1}{2} \sum_{i=1}^N \gamma_i^B \gamma_i^A + i \frac{1}{2} \sum_{i=1}^{N-1} (\omega_+ \gamma_i^B \gamma_{i+1}^A + \omega_- \gamma_{i+1}^B \gamma_i^A), \quad \text{with } \omega_\pm = \Delta \pm t \quad (15)$$

From it we can distinguish between two phases—trivial and topological—, corresponding, respectively, to two different ways of pairing these Majoranas states—no unpaired modes or one isolated mode on both edges. These pairing configuration are depicted in Fig.4 in blue and red respectively. This phases can be easily identified, respectively, in their limiting regimes where one sets $\Delta = t = 0$ and $\mu = 0$ with $\Delta = t \neq 0$.

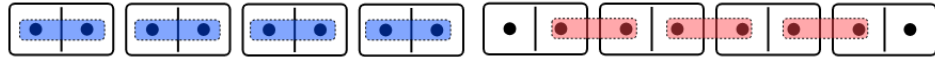


Figure 4. Kitaev chain Majorana modes pairing possibilities

Indeed, see that by setting $\Delta = t = 0$ within the Hamiltonian of Eq.(15) we obtain

$$H_{\text{trivial}} = -i\mu \frac{1}{2} \sum_{i=1}^N \gamma_i^B \gamma_i^A, \quad (16)$$

which corresponds to the limiting case of "no unpaired Majorana modes" configuration. The energy cost for each fermion to be occupied is μ , with all excitations having an energy of either $\pm\mu/2$. The band structure will then have a gapped bulk and no zero energy edge states. Furthermore, see that the wavefunctions of the first three energy states shown in Fig.(5).(middle) in this trivial phase simply resemble the harmonic modes of a string states.

On the other hand, see that by setting $\mu = 0$ with $\Delta = t \neq 0$ we obtain

$$H_{\text{topological}} = it \sum_{n=1}^{N-1} \gamma_n^B \gamma_{n+1}^A \quad (17)$$

which corresponds to the "unpaired edge Majorana mode" configuration where every Majorana operator is coupled to a Majorana operator of a different kind in the next site. Note that the summation only goes up to $n = N - 1$. Moreover, see that by assigning a new fermion operator $\tilde{c}_i = 1/2 (\gamma_i^B + i\gamma_{i+1}^A)$, the Hamiltonian can be otherwise expressed as

$$H_{\text{topological}} = 2t \sum_{n=1}^{N-1} \left(\tilde{c}_n^\dagger \tilde{c}_n + \frac{1}{2} \right) \quad (18)$$

which describes a new set of $N - 1$ Bogoliubov quasiparticles with energy t . For every Majorana pair we assign an energy difference $2t$ between the empty and filled state. All states which are not at the ends of the chain have an energy of $\pm t$ and thus the bands structure has a gapped bulk. However, see that the missing mode $\tilde{c}_N = 1/2 (\gamma_N^B + i\gamma_1^A)$, which couples the Majorana operators from the two endpoints of the chain, does not appear in the Hamiltonian and thus it most have zero energy. As the presence of this mode does not change the total energy, the ground state is two-fold degenerate. This condition is a topological superconducting non-trivial phase. This mode is called a Majorana zero mode and is highly delocalized at the edges, as it can be seen in red in Fig(5).(middle). As one tunes μ in the direction of the trivial phase, the topological gap, protected by particle-hole symmetry (PHS), gets smaller and smaller and the Majoranas wavefunctions stay less and less localized at the edges. At the transition between the trivial and topological, when the chemical potential takes it's critical value of $|\mu| = 2t$, the first energy states stays evenly distributed along the chain.

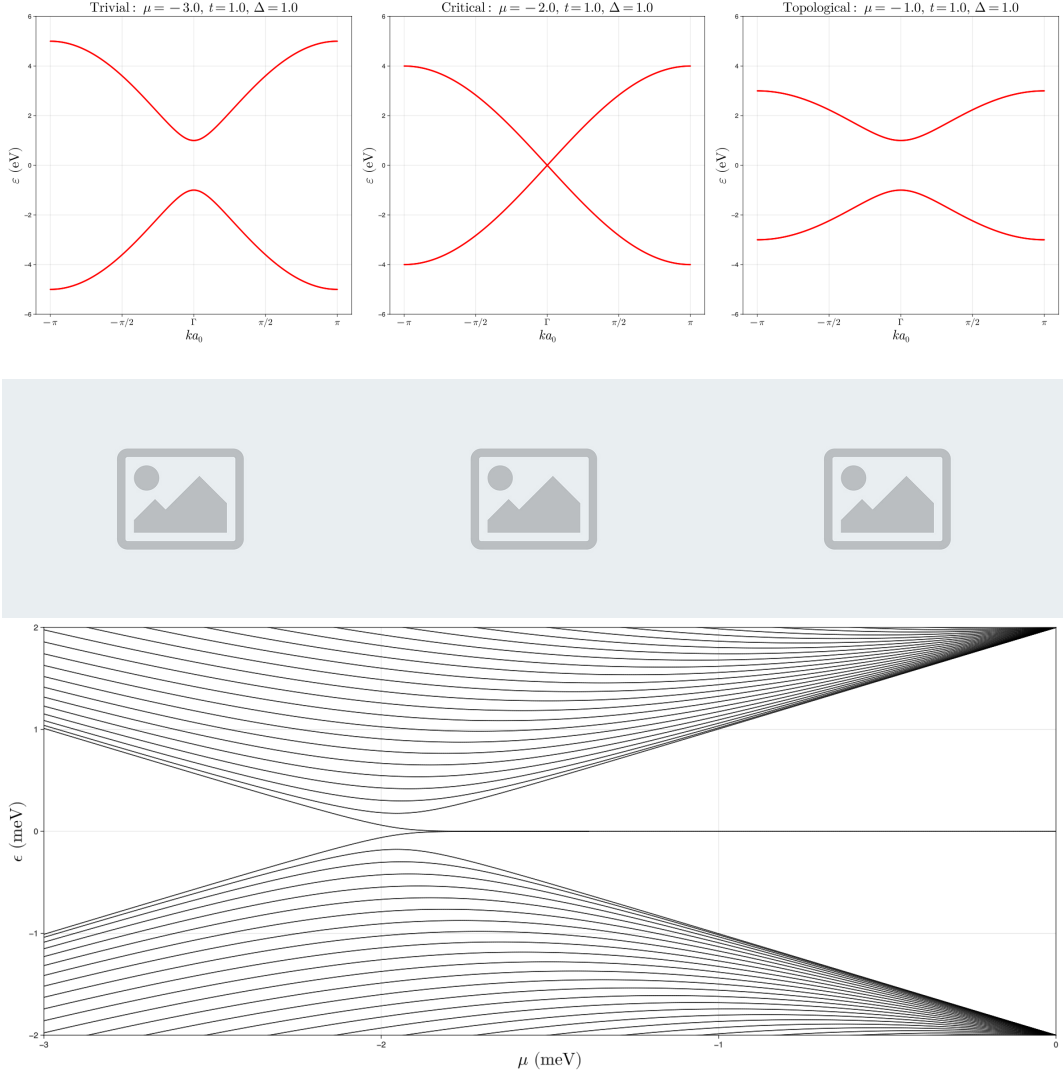


Figure 5. Kitaev chain (**top**) band structure (**middle**) I will eventually plot the 1st, 2nd and 3rd state wavefunction here at each regime, and (**bottom**) band spectrum for a chain length of $L = 50$ with lattice spacing $a_0 = 1$ fixing $\Delta = t = 1.0$. The critical μ shifts forward to infinity as $L \rightarrow 0$.

Bogoliubov-de Gennes Hamiltonian Let us now define the Hamiltonian in E.(12) in its Bogoliubov-de Gennes (BdG) form

$$H = \frac{1}{2} \check{c}^\dagger H_{\text{BdG}} \check{c}.$$

where we have defined the Nambu spinor as

$$\check{c}_i^\dagger = \begin{pmatrix} c_i^\dagger & c_i \end{pmatrix} \quad \text{and} \quad \check{c}_i = \begin{pmatrix} c_i \\ c_i^\dagger \end{pmatrix} \quad (19)$$

This proves not only useful to the study of the system's symmetries, but it also a necessary step for the numerical implementation in *Quantical.jl*. Defining τ_x, τ_y, τ_z as Pauli matrices in the particle-hole

subspace and using we the fermionic anti-commutation properties $\{c_i, c_j^\dagger\} = \delta_{ij}$ and $\{c_i, c_j\} = 0$, one can check that

$$\mu : \quad \check{c}_i^\dagger \tau_z \check{c}_i = \begin{pmatrix} c_i^\dagger & c_i \end{pmatrix} \begin{pmatrix} 1 & 0 \\ 0 & -1 \end{pmatrix} \begin{pmatrix} c_i \\ c_i^\dagger \end{pmatrix} = c_i^\dagger c_i - c_i c_i^\dagger = 2c_i^\dagger c_i - 1 \quad (20)$$

$$t : \quad \check{c}_j^\dagger \tau_z \check{c}_i = \begin{pmatrix} c_j^\dagger & c_j \end{pmatrix} \begin{pmatrix} 1 & 0 \\ 0 & -1 \end{pmatrix} \begin{pmatrix} c_i \\ c_i^\dagger \end{pmatrix} = c_j^\dagger c_i - c_j c_i^\dagger = c_j^\dagger c_i + h.c \quad (21)$$

$$\Delta : \quad \check{c}_j^\dagger i \tau_y \check{c}_i = \begin{pmatrix} c_j^\dagger & c_j \end{pmatrix} \begin{pmatrix} 0 & 1 \\ -1 & 0 \end{pmatrix} \begin{pmatrix} c_i \\ c_i^\dagger \end{pmatrix} = c_j^\dagger c_i^\dagger - c_j c_i = c_j^\dagger c_i^\dagger + h.c \quad (22)$$

Hence the Hamiltonian in Eq.(12) in its BdG form reads as

$$H = \mu \frac{1}{2} \sum_i \check{c}_i^\dagger \tau_z \check{c}_i - t \sum_{i=1}^{N-1} \check{c}_{i+1}^\dagger \tau_z \check{c}_i + \Delta \sum_{i=1}^{N-1} \check{c}_{i+1}^\dagger i \tau_y \check{c}_i \quad (23)$$

See that the Hamiltonian has particle-hole symmetry, i.e $\mathcal{P} H \mathcal{P}^{-1} = -\tau_x H^* \tau_x = -H$ with $\mathcal{P} = \tau_x \mathcal{K}$ and \mathcal{K} complex conjugation, as well as time reversal symmetry, i.e $\mathcal{T} H \mathcal{T}^{-1} = H^* = H$ with $\mathcal{T} = \mathcal{K}$ for this spinless case (for reference, $\mathcal{T} = i\sigma_y \mathcal{K}$ for a 1/2-spin system). Once again, to understand why this is the case check.

Topological invariant

1. Majorana modes at a domain wall

Consider the case where we weld together two semi-infinite nanowires with one in it's trivial phase and the other in it's trivial phase. The spacial profile of the chemical potential $\mu(x)$ would then approximately a Heaviside theta function from $|\mu_{\text{left}}| > 2t$ to $|\mu_{\text{right}}| < 2t$, forming a doping domain wall at it's center. Hamiltonian wise, one just substitutes $\mu \rightarrow \mu(x)$ directly into Eq.(12). What one obtains in this situation is a Majorana mode localized at the domain wall with its twin forming in the semi-infinite edge of the topological side.

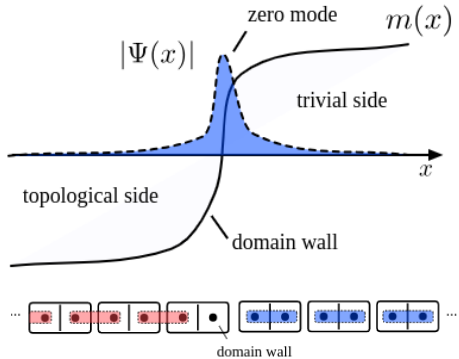


Figure 6. needs caption

2. Kitaev ring

B. SSH model

The most relevant references used for this section follow:

- Asboth's "A short course on topological insulators" - arXiv:1509.02295..
-

C. Oreg-Lutchyn model

The most relevant references used for this section follow:

- Lutchyn's "Majorana Fermions and a Topological Phase Transition in Semiconductor-Superconductor Heterostructures "- Phys. Rev. Lett. 105, 077001
 - Oreg's "Helical liquids and Majorana bound states in quantum wires" - Phys. Rev. Lett. 105, 177002
 - Lobo's "Exponential suppression of the topological gap in self-consistent intrinsic Majorana nanowires" - arXiv:2412.15174
-

The Oreg-Lutchyn Majorana minimal model consists of a finite 1D semiconductor (SM) nanowire with strong spin-orbit coupling (SOC) α and a tunable chemical potential μ , in proximity of a superconductor (SC) of homogeneous pairing Δ , having a magnetic field B_z applied along its length, defined as the \hat{z} direction. The Rashba effect describes the coupling of an electric field E_x that breaks inversion symmetry breaking in the direction perpendicular to the wire, to the electron's spin, i.e $\propto (i\vec{\nabla} \times \hat{x}) \cdot \vec{\sigma} = i\sigma_y \partial_z$ with $\vec{\sigma} = (\sigma_x, \sigma_y, \sigma_z)$. The Zeeman effect described the spin splitting due to the in-plane magnetic field B_z . The pairing term describes the Cooper pairs from BCS theory than could tunnel from the SM to the SC.

The tight-binding Hamiltonian describing such system can then be decomposed as

$$H = H_K + H_{SOC} + H_Z + H_{SC} \quad (24)$$

$$H_K = (2t - \mu) \sum_{i\sigma} c_{i\sigma}^\dagger c_{i\sigma} - t \sum_{\langle i,j \rangle \sigma} c_{i\sigma}^\dagger c_{j\sigma} \quad (25)$$

$$H_{SOC} = \frac{\alpha}{2a_0} \sum_{i\sigma} (c_{i+1\bar{\sigma}}^\dagger c_{i\sigma} + h.c.) \quad (26)$$

$$H_Z = V_Z \sum_i (c_{i\uparrow}^\dagger c_{i\uparrow} - c_{i\downarrow}^\dagger c_{i\downarrow}) \quad (27)$$

$$H_{SC} = \Delta (c_{i\downarrow}^\dagger c_{i\uparrow}^\dagger + h.c.) \quad (28)$$

with c_i^\dagger (c_i) fermionic creation (annihilation) operators, μ the chemical potential, $t = \eta/a_0^2$ the hopping energy into $\langle i, j \rangle$ nearest-neighbouring sites with a_0 the lattice constant and $\eta = \hbar^2/2m^*$ with m^* the effective mass of the electrons, $V_Z = g_J \mu_B B_z / 2$ the Zeeman potential with g_J the Landé gyromagnetic moment and μ_B Bohr's magneton, α the Rashba SOC strength and Δ proximity induced superconducting s -wave pairing.

A paragraph explaining the bands.

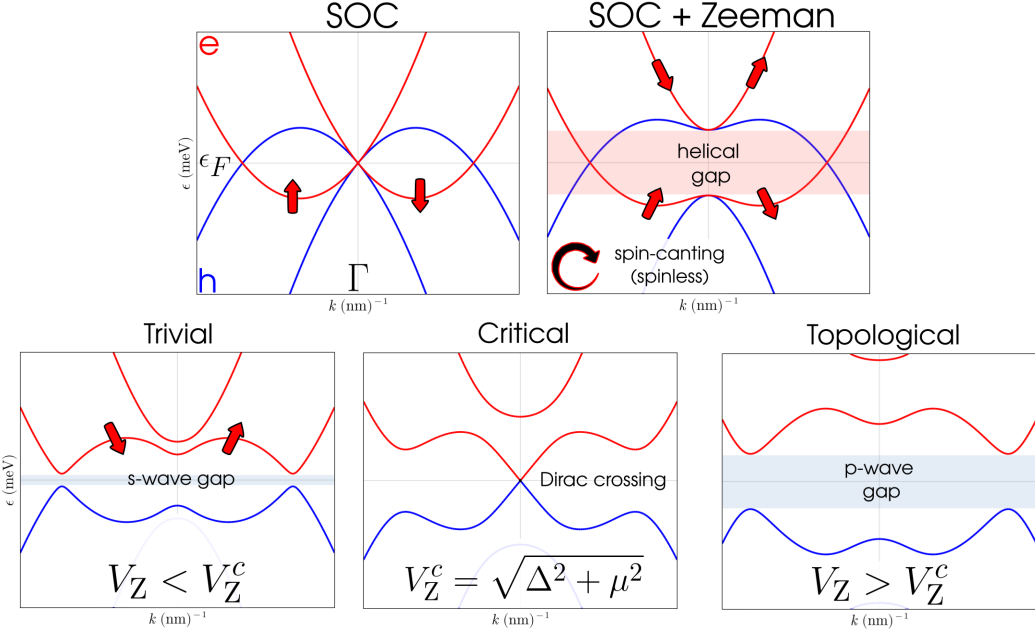


Figure 7.

A paragraph explaining the phase-diagram, pfaffian and band spectrum.

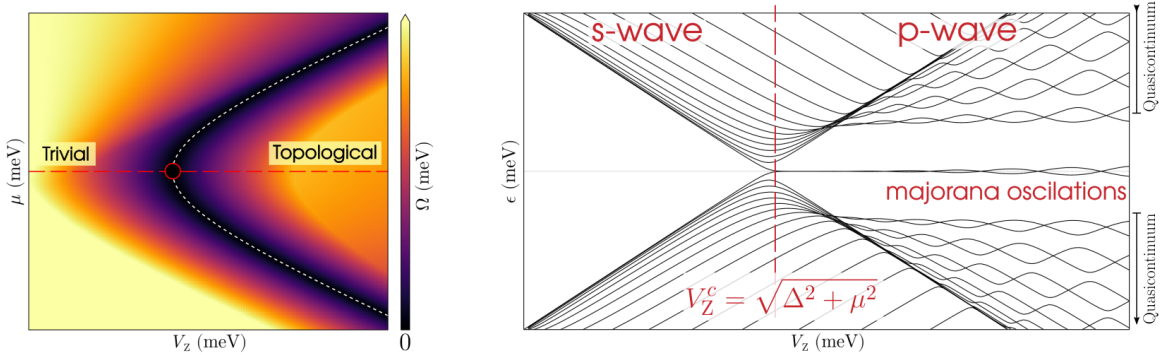


Figure 8.

Bogoliubov-de Gennes Hamiltonian Shown below are the broad strokes of a numerical implementation of the Hamiltonian in Julia using the Quantica.jl. However, prior to this implementation, we will be needing the Bogoliubov-de Gennes formalism. For this, need to double the degrees of freedom through the Nambu-spinor. In the so called unrotated-spin basis we define a Nambu spinor as

$$\check{c}_i^\dagger = \begin{pmatrix} c_i^\dagger & c_i \end{pmatrix} = \begin{pmatrix} c_{i\uparrow}^\dagger & c_{i\downarrow}^\dagger & c_{i\uparrow} & c_{i\downarrow} \end{pmatrix} \quad (29)$$

In this Nambu \otimes spin orbital space the Hamiltonian in Eq.(24) reads

$$H = H_K + H_{SOC} + H_Z + H_{SC} \quad (30)$$

$$H_K = (2t - \mu) \sum_i \check{c}_i^\dagger [\tau_z \otimes \sigma_0] \check{c}_i - \frac{1}{2} t \sum_{\langle i,j \rangle} \check{c}_i^\dagger [\tau_z \otimes \sigma_0] \check{c}_j \quad (31)$$

$$H_{SOC} = \frac{\alpha}{2a_0} \sum_i \check{c}_i^\dagger [\tau_z \otimes i\sigma_y] \check{c}_{i+1} \quad (32)$$

$$H_Z = V_Z \sum_i \check{c}_i^\dagger [\tau_z \otimes \sigma_z] \check{c}_i \quad (33)$$

$$H_{SC} = \frac{1}{2} \Delta \sum_i \check{c}_i^\dagger [\tau_y \otimes \sigma_y] \check{c}_i \quad (34)$$

with τ Pauli matrices in the particle-hole subspace and σ in the spin subspace.

To understand why this is the case check we show explicitly the derivation for the pairing term as an example. It reads:

$$\begin{aligned} \check{c}^\dagger [\tau_y \otimes \sigma_y] \check{c} &= \left(\begin{array}{cccc} c_\uparrow^\dagger & c_\downarrow^\dagger & c_\uparrow & c_\downarrow \end{array} \right) \left(\begin{array}{cc|cc} 0 & 0 & 0 & -1 \\ 0 & 0 & +1 & 0 \\ \hline 0 & +1 & 0 & 0 \\ -1 & 0 & 0 & 0 \end{array} \right) \left(\begin{array}{c} c_\uparrow \\ c_\downarrow \\ c_\uparrow \\ c_\downarrow \end{array} \right) \\ &= -c_\uparrow^\dagger c_\downarrow^\dagger + c_\downarrow^\dagger c_\uparrow^\dagger + c_\uparrow c_\downarrow - c_\downarrow c_\uparrow = 2 (c_\downarrow^\dagger c_\uparrow^\dagger + \text{h.c.}) \end{aligned} \quad (35)$$

where we the fermionic anti-commutation properties $\{c_i, c_j^\dagger\} = \delta_{ij}$ and $\{c_i, c_j\} = 0$.

The remaining terms derivation is analogous but even simpler because there is will be no mixing of particle with particle-hole components; the holeonic terms will correspond to the negative of the electronic terms, meaning that one just needs to expand the space according to $\tau_z \otimes$ the respective spin matrix. For the kinetic term there is no mixing of spin so it must trivially have the spin Pauli matrix σ_0 . Similarly, for the Zeeman term there is only the same-spin mixing of the type $\uparrow\uparrow - \downarrow\downarrow$ so it must have σ_z . As for the SOC term there is spin-mixing of opposing spins, so the options are either σ_x or $i\sigma_y$ (with a i for it to be hermitian). One can check with the fermionic anti-commutation properties that it is indeed $i\sigma_y$.

Alternative Nambu basis It is common for people to define instead the Nambu spinor in a rotated basis as such

$$\bar{c}_i^\dagger = \left(\begin{array}{c} c_i^\dagger \\ [i\sigma_y c_i] \end{array} \right) = \left(\begin{array}{cc} c_{i\uparrow}^\dagger & c_{i\downarrow}^\dagger \\ \hline c_{i\downarrow} & -c_{i\uparrow} \end{array} \right) \quad (36)$$

As also explained in section II.C.1 of the previous part, these basis' operators relate to each other as

$$\bar{c}_i = \bar{\mathcal{U}} \check{c}_i \Leftrightarrow \check{c}_i = \bar{\mathcal{U}}^\dagger \bar{c}_i \quad (37)$$

$$\bar{c}_i^\dagger = \check{c}_i^\dagger \bar{\mathcal{U}}^\dagger \Leftrightarrow \check{c}_i^\dagger = \bar{c}_i^\dagger \bar{\mathcal{U}} \quad (38)$$

and, consequently, for a generic \check{M} matrix,

$$\bar{M} = \bar{\mathcal{U}} \check{M} \bar{\mathcal{U}}^\dagger \quad (39)$$

with $\bar{\mathcal{U}}$ is a unitary matrix (i.e $\bar{\mathcal{U}}^\dagger \bar{\mathcal{U}} = \bar{\mathcal{U}} \bar{\mathcal{U}}^\dagger = \mathbb{1}$)

$$\bar{\mathcal{U}} = \begin{pmatrix} \sigma_0 & 0 \\ 0 & \imath\sigma_y \end{pmatrix} \quad (40)$$

Making use of Pauli matrices' property

$$\sigma_\alpha \sigma_\beta = \sigma = \sigma_0 \delta_{\alpha\beta} + i \varepsilon_{\alpha\beta\gamma} \sigma_\gamma \quad (41)$$

one can check that

$$H_K : \bar{\mathcal{U}} [\tau_z \otimes \sigma_0] \bar{\mathcal{U}}^\dagger = [\tau_z \otimes \sigma_0] \quad (42)$$

$$H_{SOC} : \bar{\mathcal{U}} [\tau_z \otimes \imath\sigma_y] \bar{\mathcal{U}}^\dagger = [\tau_z \otimes \imath\sigma_y] \quad (43)$$

$$H_Z : \bar{\mathcal{U}} [\tau_z \otimes \sigma_z] \bar{\mathcal{U}}^\dagger = [\tau_z \otimes \sigma_z] \quad (44)$$

$$H_{SC} : \bar{\mathcal{U}} [\tau_y \otimes \sigma_y] \bar{\mathcal{U}}^\dagger = [\tau_x \otimes \sigma_0] \quad (45)$$

meaning that, in this the rotated basis, only the pairing Hamiltonian has it's Pauli matrices changed. Concretely,

$$H_{SC} = \frac{1}{2} \Delta \sum_i \bar{c}_i^\dagger [\tau_x \otimes \sigma_0] \bar{c}_i \quad (46)$$

VII. QUANTUM HALL EFFECTS

A. Integer quantum Hall effect

B. Quantum spin Hall (Kane-Mele) effect

C. Quantum anomalous Hall effect

D. Fraction Hall effect

VIII. GRAPHENE

A. Monolayer graphene

Hexagonal boron nitride (hBN) is a 2D material composed of a simple layer of alternating boron and nitrogen atoms disposed in a planar honeycomb lattice, as shown in Fig.(10)(a). The Bravais lattice

$$\mathbf{r}_i = n_{i1} \mathbf{a}_1 + n_{i2} \mathbf{a}_2, \quad n_{i1}, n_{i2} \in \mathbb{Z} \quad (47)$$

is generated by the real vectors basis

$$\mathbf{a}_1 = a_0 \begin{bmatrix} +\sin(30^\circ) \\ +\cos(30^\circ) \end{bmatrix} \text{ and } \mathbf{a}_2 = a_0 \begin{bmatrix} +\sin(30^\circ) \\ -\cos(30^\circ) \end{bmatrix}. \quad (48)$$

where $\sin(30^\circ) = 1/2$ and $\cos(30^\circ) = \sqrt{3}/2$. In each diamond shaped Wigner-Seitz primitive cell (depicted in yellow), we have one boron atom and one nitride atom, which we designate as sub-lattices

A (depicted in red) and B (depicted in blue) respectively. The atoms within the central primitive cell are located at

$$\mathbf{s}_A = \frac{a_0}{\sqrt{3}} \begin{bmatrix} 0 \\ -1/2 \end{bmatrix} \text{ and } \mathbf{s}_B = \frac{a_0}{\sqrt{3}} \begin{bmatrix} 0 \\ +1/2 \end{bmatrix}. \quad (49)$$

where the origin is defined at the midpoint between the atoms. For each site A , the position of the nearest-neighbors (NN) in the sites B are given by

$$\boldsymbol{\delta}_1 = \frac{a_0}{\sqrt{3}} \begin{bmatrix} 0 \\ 1 \end{bmatrix}, \boldsymbol{\delta}_2 = \frac{a_0}{\sqrt{3}} \begin{bmatrix} +\sin(60^\circ) \\ -\cos(60^\circ) \end{bmatrix} \text{ and } \boldsymbol{\delta}_3 = \frac{a_0}{\sqrt{3}} \begin{bmatrix} -\sin(60^\circ) \\ -\cos(60^\circ) \end{bmatrix}. \quad (50)$$

where $\sin(60^\circ) = \sqrt{3}/2$ and $\cos(60^\circ) = 1/2$. All these vectors are shown in Fig.(10)(a) within the real space lattice. Furthermore, from the real lattice basis vectors, in order to fulfill $\mathbf{a}_i \cdot \mathbf{b}_j = 2\pi\delta_{ij}$, the reciprocal lattice basis vectors follow as

$$\mathbf{b}_1 = \frac{2\pi}{a_0} \begin{bmatrix} +\cos(30^\circ) \\ -\sin(30^\circ) \end{bmatrix} \text{ and } \mathbf{b}_2 = \frac{2\pi}{a_0} \begin{bmatrix} +\cos(30^\circ) \\ +\sin(30^\circ) \end{bmatrix}. \quad (51)$$

These are also shown in Fig.(10)(b) together with the first zone of Brillouin, formed by the area enclosed by the intersection of their bisectrices. The high-symmetry points are Γ , the origin, the Dirac points K_\pm and M read as

$$\boldsymbol{\Gamma} = \begin{bmatrix} 0 \\ 0 \end{bmatrix}, \quad K_\pm = \pm \frac{4\pi}{3a_0} \begin{bmatrix} 1 \\ 0 \end{bmatrix} \text{ and } M = \frac{2\pi}{a_0} \begin{bmatrix} +\cos(30^\circ)/2 \\ +\sin(30^\circ)/2 \end{bmatrix} \quad (52)$$

where the K point is found such that $(\mathbf{M} + K_{k_x} \hat{\mathbf{M}}_\perp)_{k_y} = 0$, with $\hat{\mathbf{M}}_\perp$ the unit vector in the perpendicular direction to \mathbf{M} . In far right side of Fig.(9), we make a note that the discretized grid it's in the Bloch momentums basis $\{\phi_1, \phi_2\}$, i.e in the direction of the reciprocal lattice vectors, and not simply in the reciprocal space $\{k_x, k_y\}$. In the Bloch momentums basis the Dirac points would reads as $K_\pm = 2\pi/3a_0 [\pm 1, \mp 1]$.

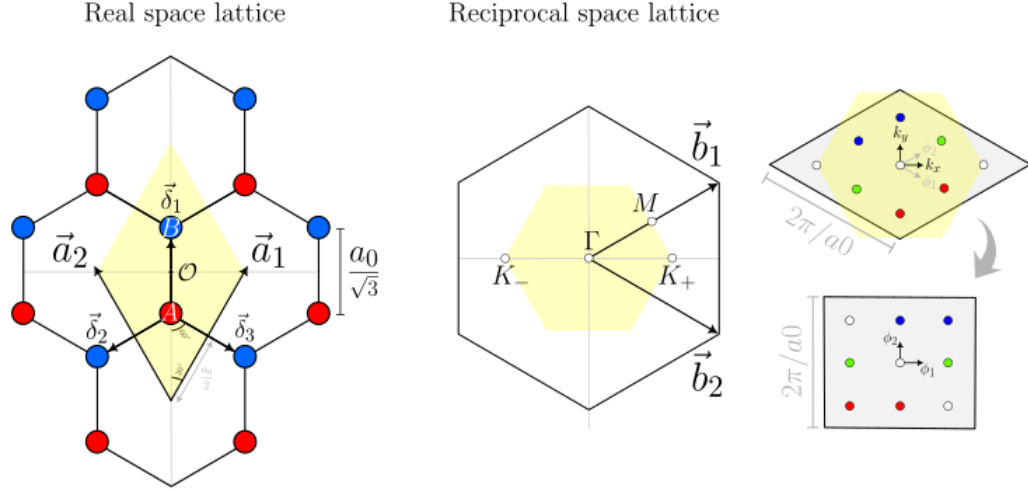


Figure 9.

Let us consider the nearest-neighbors (NN) tight-binding model, written in real space as

$$H_{\text{TB}}(\mathbf{R}) = \sum_i \epsilon_A a_{\mathbf{r}_i}^\dagger a_{\mathbf{r}_i} + \sum_i \epsilon_B b_{\mathbf{r}_i}^\dagger b_{\mathbf{r}_i} - t \sum_{\langle i,j \rangle} (a_{\mathbf{r}_i}^\dagger b_{\mathbf{r}_i+\delta_j} + b_{\mathbf{r}_j}^\dagger a_{\mathbf{r}_i-\delta_j}), \quad (53)$$

where the operators $a_{\mathbf{r}_i}^\dagger (a_{\mathbf{r}_i})$ create (annihilate) an electron in the sub-lattice A in a given Bravais lattice site \mathbf{r}_i , the operators $b_{\mathbf{r}_i}^\dagger (b_{\mathbf{r}_i})$ the same but for sub-lattice B , ϵ_A and ϵ_B are the onsite energies of site A and B respectively, and t is the hopping strength between nearest-neighbouring sites A and B and back, denoted with $\langle i,j \rangle$.

Expressing the creation/annihilation operators as their Fourier counterparts,

$$a_{\mathbf{R}_i} = \frac{1}{\sqrt{V}} \sum_{\mathbf{k}} e^{i\mathbf{k}\cdot(\mathbf{R}_i+\mathbf{s}_A)} a_{\mathbf{k}} \quad \text{and} \quad b_{\mathbf{R}_i} = \frac{1}{\sqrt{V}} \sum_{\mathbf{k}} e^{i\mathbf{k}\cdot(\mathbf{R}_i+\mathbf{s}_B)} b_{\mathbf{k}}, \quad (54)$$

and using the identity $\delta(\mathbf{k} - \mathbf{k}') = 1/N \sum_i e^{-i\mathbf{R}_i \cdot (\mathbf{k} - \mathbf{k}')}$, we obtain the Hamiltonian in reciprocal space,

$$H_{\text{TB}}(\mathbf{R}) = \sum_{\mathbf{k}} \epsilon_A a_{\mathbf{k}}^\dagger a_{\mathbf{k}} + \sum_{\mathbf{k}} \epsilon_B b_{\mathbf{k}}^\dagger b_{\mathbf{k}} - t \sum_{\mathbf{k}} (\gamma_{\mathbf{k}} a_{\mathbf{k}}^\dagger b_{\mathbf{k}} + \gamma_{\mathbf{k}}^\dagger b_{\mathbf{k}}^\dagger a_{\mathbf{k}}), \quad (55)$$

where $\gamma_{\mathbf{k}} = \sum_{\langle j \rangle} \exp(+i\mathbf{k} \cdot \boldsymbol{\delta}_j)$ is complex number. If we now define a row vector $c_{\mathbf{k}}^\dagger = [a_{\mathbf{k}}^\dagger \ b_{\mathbf{k}}^\dagger]$ we can rewrite the system's Hamiltonian as $H_{\mathbf{R}}^{\text{TB}} = \sum_{\mathbf{k}} c_{\mathbf{k}}^\dagger H_{\mathbf{k}}^{\text{TB}} c_{\mathbf{k}}$ with

$$H_{\text{TB}}(\mathbf{k}) = \begin{bmatrix} \epsilon_A & -t\gamma_{\mathbf{k}} \\ -t\gamma_{\mathbf{k}}^\dagger & \epsilon_B \end{bmatrix}. \quad (56)$$

Within this simplified tight-binding model, the expression for the electronic two-band structure can easily be obtained analytically by diagonalizing the matrix in Eq.(56), yielding

$$E_{\text{TB}}^{\pm}(\mathbf{k}) = \pm \sqrt{\epsilon^2 + t^2 \left[3 + 2 \cos(a_0 k_x) + 4 \cos\left(\frac{a_0 \sqrt{3}}{2} k_y\right) \cos\left(\frac{a_0}{2} k_x\right) \right]}, \quad (57)$$

having defined the zero point energy at $(\epsilon_A + \epsilon_B)/2$ and defined $\epsilon \equiv (\epsilon_A - \epsilon_B)/2$ at the middle of the gap such that $\epsilon_A = \epsilon$ and $\epsilon_B = -\epsilon$. The valence band corresponds to the $E_{\text{TB}}^-(\mathbf{k})$ dispersion while the $E_{\text{TB}}^+(\mathbf{k})$ corresponds to the conduction band, as shown in Fig.(10)(c). The band structure is accompanied by the density of states $\text{DoS}(E) = \sum_{\mathbf{k}} \delta(E - E(\mathbf{k}))$.

Notice that, if $\epsilon_A = \epsilon_B$, as is the case for graphene, we obtain $\epsilon = 0$ and the band dispersion closes in a linear fashion at the so called Dirac points. In hBN, the electronic band dispersion is also at its minimum near these points but has instead a parabolic shape. In either case, this points represent a fundamental symmetry of the system, called valley parity. To see why the dispersion is parabolic at these valley points, we Taylor series expand the exponential of $\gamma_{\mathbf{k}}$ in Eq.(??) near $\mathbf{k} \rightarrow \mathbf{K} + \mathbf{p}$ with $\mathbf{p} \rightarrow 0$. We obtain $\exp(+i\mathbf{p} \cdot \boldsymbol{\delta}_j) \approx 1 + i\mathbf{p} \cdot \boldsymbol{\delta}_j$. Now, since $\sum_{\langle j \rangle} \exp(+i\mathbf{K} \cdot \boldsymbol{\delta}_j) = 0$ we are left with $\gamma_{\mathbf{K}+\mathbf{p}} \simeq i\mathbf{p} \cdot \sum_{\langle j \rangle} \exp(+i\mathbf{K} \cdot \boldsymbol{\delta}_j) \boldsymbol{\delta}_j = -\sqrt{3}a_0/2(p_x - ip_y)$. Invoking the Pauli matrices definitions, from Eq.(56) we can write the TB Hamiltonian $H_{\text{TB}}^{\mathbf{k}}$ in this low-energy regime as

$$H_{\text{TB}}(\mathbf{K} + \mathbf{p}) = \epsilon \sigma_z + t \frac{\sqrt{3}a_0}{2} (\mathbf{p} \cdot \boldsymbol{\sigma}), \quad (58)$$

which clearly resembles the 2D Dirac Hamiltonian, $H_{\text{Dirac}} = \sigma_z mc^2 + c(\mathbf{p} \cdot \boldsymbol{\sigma})$ with ϵ taking the role of the rest mass energy mc^2 and instead with a velocity $v_F = t\sqrt{3}a_0/2$, termed the *Fermi velocity*, as a

replacement to the velocity of light c . Notice that, for the case of graphene, since $\epsilon = 0$, the electrons would behave as if they are massless. In this limit, the hBN low-energy dispersion can be written as the typical relativistic dispersion relation

$$E_{\text{TB}}(\mathbf{K} + \mathbf{p}) = \pm \sqrt{p^2 v_F^2 + m_{\text{eff}}^2 v_F^4}. \quad (59)$$

where m_{eff} is the effective mass of the electron at a given point near the valleys.

Refazer esta figura em Quantica para aprender a fazer densidade de estados. Falar das singularidades de van Hove.

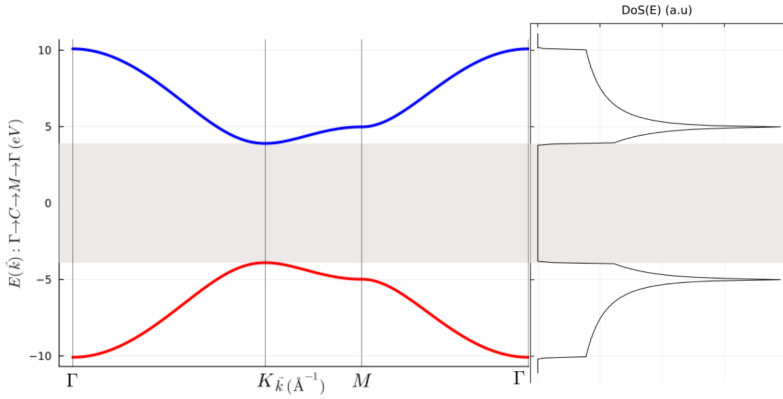


Figure 10. hBN electronic band structure from a nearest-neighbor tight-binding model accompanied by the density of the states. The dispersion goes along the symmetry path $\mathbf{k} : \Gamma \rightarrow K \rightarrow M \rightarrow \Gamma$ and was calculated using $\epsilon_g = 7.8\text{eV}$ for the energy gap, $t = 3.1\text{eV}$ for the hopping parameter and $a_0 = 1.42\sqrt{3}\text{\AA}$ for the honeycomb lattice length.

B. Haldane model

C. Bilayer Bernal graphene

Consider a bilayer graphene model depicted in Fig.(11).

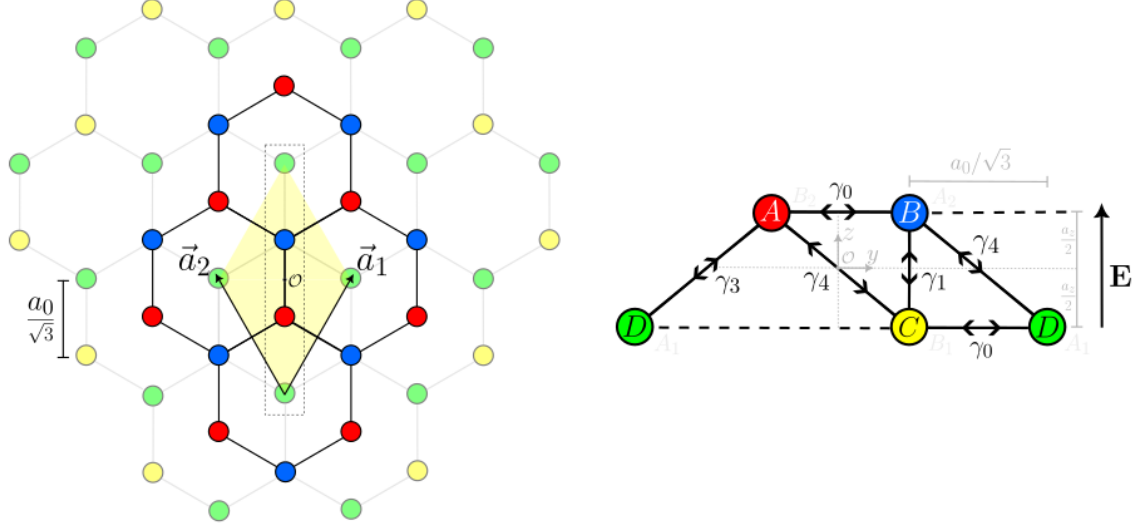


Figure 11. (a) Top view of the bilayer graphene (b) Side view of the dotted region in (a)

The tight-binding Hamiltonian of such a model reads

$$\begin{aligned}
 H_{\text{BLG}} &= H_{\text{intralayer}} + H_{\text{interlayer}} = (H_{\text{top}} + H_{\text{bot}}) + (H_{\gamma_1} + H_{\gamma_3} + H_{\gamma_4}) \\
 H_{\text{top}} &= \sum_i (\epsilon_A - \mu) c_i^\dagger a_i + \sum_i (\epsilon_B - \mu) b_i^\dagger b_i - \gamma_0 \sum_{\langle i,j \rangle} (a_i^\dagger b_j + h.c.) \\
 H_{\text{bot}} &= \sum_i (\epsilon_C - \mu) c_i^\dagger c_i + \sum_i (\epsilon_D - \mu) d_i^\dagger d_i - \gamma_0 \sum_{\langle i,j \rangle} (c_i^\dagger d_j + h.c.) \\
 H_{\gamma_1} &= +\gamma_1 \sum_{\langle i,j \rangle} (b_i^\dagger c_j + h.c.) \\
 H_{\gamma_3} &= -\gamma_3 \sum_{\langle i,j \rangle} (a_i^\dagger d_j + h.c.) \\
 H_{\gamma_4} &= +\gamma_4 \sum_{\langle i,j \rangle} (b_i^\dagger d_j + h.c.) + t_4 \sum_{\langle i,j \rangle} (a_i^\dagger C_j + h.c.)
 \end{aligned}$$

Here, a site located at \mathbf{r}_i is indexed by the side index i and its next nearest neighbors located at \mathbf{r}_j are indexed with the site index j . Of course, \mathbf{r}_j depends on the kind of hopping in question: for γ_0 it's $\mathbf{r}_j = \mathbf{r}_i + \boldsymbol{\delta}_j$ with $j = 1, 2, 3$, for γ_1 it's $\mathbf{r}_j = \mathbf{r}_i \pm a_z \hat{\mathbf{z}}$, and for γ_3 and γ_4 it's $\mathbf{r}_j = \mathbf{r}_i + \boldsymbol{\delta}_j \pm a_z \hat{\mathbf{z}}$. Moreover, let us consider an electric field \mathbf{E} uniform in the plane xOy and growing along the $\hat{\mathbf{z}}$, described by the tight-binding Hamiltonian

$$H_E = \sum_i E_i (f_{i\uparrow}^\dagger f_{i\uparrow} - f_{i\downarrow}^\dagger f_{i\downarrow})$$

where $E_i = E \times z_i$ is the amplitude of the electric field at position \mathbf{r}_i , only really dependent on z_i , and $f_i^\dagger = [f_{i\uparrow}^\dagger \ f_{i\downarrow}^\dagger]$ is a generic fermionic operator. Since in our bilayer model the bottom layer is situated at $z = 0$ we redefine $E(a_z) = E$, such that

$$H_{\text{BLG}+} = E \sum_i \left\{ (a_{i\uparrow}^\dagger a_{i\uparrow} - a_{i\downarrow}^\dagger a_{i\downarrow}) + (b_{i\uparrow}^\dagger b_{i\uparrow} - b_{i\downarrow}^\dagger b_{i\downarrow}) \right\}$$

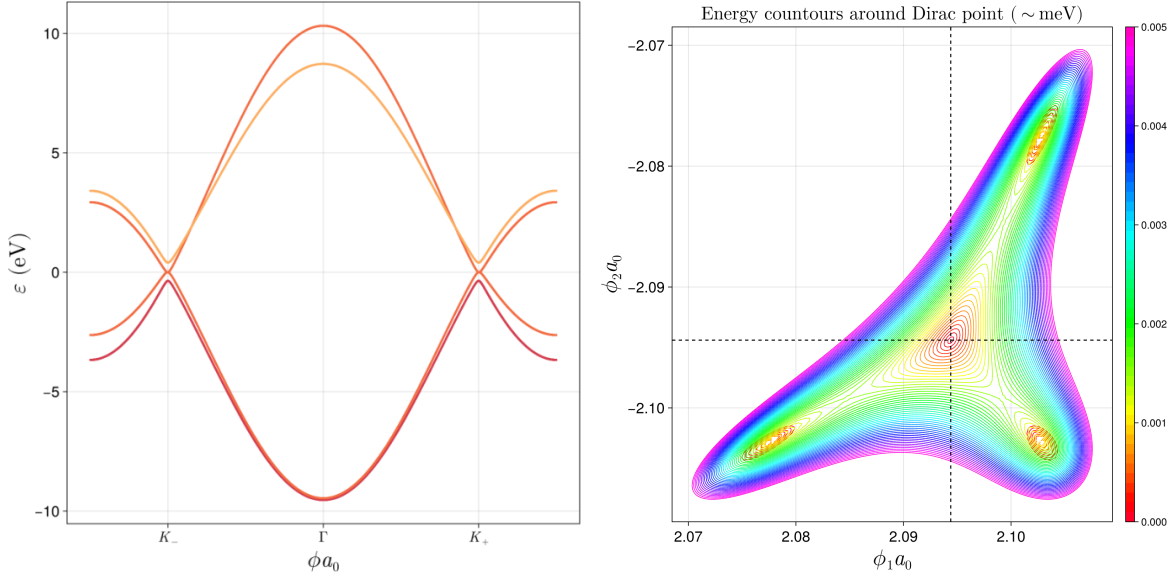


Figure 12. (a, b) Bandstructure along symmetry path $\Gamma \rightarrow K_+ \rightarrow M$ and (c) trigonal warping of BLG around the Dirac point K_+ .

1. Armchair and Zigzag configurations

D. Kekulé modulation

E. Twisted bilayer graphene